ISBN: 978-628-95207-4-3. ISSN: 2414-6390. Digital Object Identifier: 10.18687/LACCEI2023.1.1.1438

Effect of the Substitution of Co by Ni on the Crystal Structure and Magnetic Properties of Cobalt Ferrite Nanoparticles

Gerson Márquez, Ph.D.[1,2], and Vicente Sagredo, M.Sc.[2]
[1]Universidad Tecnológica del Perú, Perú, gmarquez@utp.edu.pe
[2]Universidad de Los Andes, Venezuela, visesaar@gmail.com

Abstract*– $Ni_{1-x}Co_xFe_2O_4$ (x = 1.0, 0.8, 0.6, and 0.5) nanoparticles were synthesized using the coprecipitation method and subsequent thermal treatment at 800 °C. The structural characterization of the nanoparticles was carried out using X-ray Diffraction, finding that all the compounds presented a single crystalline phase corresponding to the cubic spinel structure. As the concentration of Ni in the compounds increases, a decrease in the lattice parameter was obtained because of the fact that Ni^{2+} cations are smaller than Co^{2+}. The size, morphology and dispersion of the nanoparticles were analyzed by Transmission Electron Microscopy, finding that the nanocompounds are formed by aggregates of nanoparticles with irregular shapes and mean particle sizes between 34 and 42 nm. The magnetic properties of $CoFe_2O_4$ and $Co_{0.5}Ni_{0.5}Fe_2O_4$ nanoparticles were studied from magnetization measurements as a function of temperature, in ZFC and FC modes, and magnetization measurements as a function of the applied magnetic field. It was obtained that the nanoparticles are in the blocked magnetic regime in the temperature range from 5 to 320 K. At 5 K, the compounds have large coercive fields of 10683 and 7518 Oe, for $CoFe_2O_4$ and $Co_{0.5}Ni_{0.5}Fe_2O_4$, respectively. It was found that the values of saturation magnetization, remanent magnetization, and coercive field decrease when replacing Co^{2+} by Ni^{2+} in Co ferrite, because the magnetic moments of divalent nickel cations are smaller than those of Co^{2+} cations.

Keywords*-- nanoparticles, ferrite, coprecipitation, spinel, magnetization.

I. Introduction

Ferrites are magnetic oxides of iron and other chemical elements that have high magnetic permeability and low electrical conductivity, making them useful materials for absorbing high-frequency energy, which is why they are used as transformer cores, inductors, and filters to absorb and eliminate unwanted signals or radio frequency interference in circuits [1]–[3]. Ferrites are materials with a great response and sensitivity in the presence of magnetic fields, which has allowed them to be used to detect the intensity and direction of magnetic fields generated by electric motors and other devices [4]. As nanoparticles, ferrites can present unique and interesting properties such as large surface area and superparamagnetism at room temperature, so they can be used in a wide variety of applications such as ferrofluids and nanopowders for use in catalysis and environmental remediation, removing contaminants such as heavy metals in wastewater [5]–[7]. Furthermore, ferrite nanoparticles are used in biomedical applications such as the detection of biomolecules, cells, and viruses; as contrast agents for magnetic resonance imaging, and in magnetic therapy for cancer treatment, eliminating cancerous tumors taking advantage of the heating generated by the energy dissipated by the nanoparticles in the relaxation process that they experience under the application of alternating magnetic fields [8], [9].

Cubic ferrites have the formula MFe_2O_4, where M is a divalent cation, and they crystallize in the spinel structure, which has two types of interstitial sites in which the ions are located. These sites have tetrahedral and octahedral coordination, and the M^{2+} and Fe^{3+} cations can be distributed between both structural positions, giving the possibility to many configurations between two extreme situations known as normal spinel and inverse spinel. In the normal spinel all the divalent cations are in the tetrahedral sites, while all the Fe^{3+} cations are in the octahedral positions. On the other hand, in the inverse spinel, half of the trivalent cations are in the tetrahedral sites and the other half, together with the M^{2+} cations, are in the octahedral positions [10]. Ferrites such as $FeFe_2O_4$ and $NiFe_2O_4$ crystallize in the inverse spinel structure, while cobalt ferrite ($CoFe_2O_4$) is partially inverse spinel with 60 - 90 % of the Co^{2+} cations located in the octahedral sites [11].

Cobalt ferrite is an interesting magnetic material that presents unusual properties such as: high magnetocrystalline anisotropy, high coercive field, moderate saturation magnetization, great chemical stability, and high mechanical hardness [10]. As a bulk material, cobalt and nickel ferrites are ferrimagnetic, with Curie temperatures of approximately 790 and 858 K, respectively; while, in the form of nanoparticles, both ferrites present superparamagnetism at room temperature, if the particles have sizes smaller than 14 nm, in $CoFe_2O_4$, and 28 nm, in $NiFe_2O_4$ [12], [13].

The synthesis method used to produce the nanoparticles can significantly influence characteristics and properties such as the shape, size, dispersion, stability, purity, and crystalline structure of the nanoparticles. Therefore, it is important to make a good selection of the appropriate synthesis method according to the desired properties and applications. Various methods have been used for the synthesis of ferrite nanoparticles, such as: coprecipitation [14], sol-gel [15], autocombustion [16], hydrothermal synthesis [17], microemulsion [18], reverse micelles [19]. Chemical coprecipitation has proven to be a simple, fast, and low-cost synthesis method that allows obtaining nanoparticulate powders [20].

Digital Object Identifier: (only for full papers, inserted by LACCEI).
ISSN, ISBN: (to be inserted by LACCEI).
DO NOT REMOVE

By replacing Co^{2+} cations with Ni^{2+} in cobalt ferrite, changes in the cation distribution occur at the tetrahedral and octahedral sites of the spinel structure, due to differences in the inversion degrees of $CoFe_2O_4$ and $NiFe_2O_4$. This, in addition to the difference between the cationic magnetic moments of Co^{2+} (3 μ_B) and Ni^{2+} (2 μ_B), should generate changes in the magnetic properties of the compounds. Therefore, we have considered it interesting to study the changes in the structural and magnetic properties, when Co^{2+} is replaced by Ni^{2+} in cobalt ferrite nanoparticles.

In the present investigation, the coprecipitation method was used to synthesize $CoFe_2O_4$, $Co_{0.8}Ni_{0.2}Fe_2O_4$, $Co_{0.6}Ni_{0.4}Fe_2O_4$ and $Co_{0.5}Ni_{0.5}Fe_2O_4$ nanoparticles. We report the crystalline structure, size, dispersion, and magnetic properties of the synthesized nanoparticles. In addition, we analyze the effect of replacing Co^{2+} by Ni^{2+} on the structural and magnetic properties of Co ferrite nanoparticles.

II. Experiment

A. *Synthesis of Nanoparticles*

$Co_{1-x}Ni_xFe_2O_4$ (x = 0.0, 0.2, 0.4, 0.5) nanoparticles were synthesized by the coprecipitation method, using cobalt(II) nitrate hexahydrate, nickel(II) nitrate hexahydrate, and iron(III) nitrate nonahydrate as metal precursors, and ammonium hydroxide (29.66 wt% in water) as the precipitating agent. The synthesis procedure described in [20] was followed. To improve the crystallinity of the nanoparticles, the obtained powders were heat treated at 800 °C, for 2 hours, in a tubular furnace with an air atmosphere. The thermal treatment was carried out by heating the samples up to the calcination temperature, with a heating rate of 1 °C/min, while the cooling was achieved spontaneously by letting the calcined powders cool down to room temperature.

B. *Characterization Techniques*

The structural characterization of the nanoparticles was performed from X-ray diffraction (XRD) data, measured in a Philips powder diffractometer, with CuKα radiation in the range $15 \leq 2\theta \leq 80°$ range, with steps of 0.05° and measurement time of 10 s/step. The analysis and processing of the XRD data was carried out using the FullProf Suite software, identifying the crystalline phases present after comparing the diffraction peaks observed with the Powder Diffraction File (PDF) database. The crystal lattice parameters were determined by the Le Bail refinement method.

The size, morphology and aggregation of the nanoparticles were determined from transmission electron microscopy (TEM) images taken using a JEOL JEM 1220 microscope, operating with an accelerating voltage of 100 kV, which allowed obtaining micrographs with a magnification of x40k. Powder samples were prepared by wet method, dispersing a small amount of material in ethanol; then, a drop of the nanoparticle suspension was placed on a carbon-coated copper grid, allowing the ethanol to evaporate until the nanoparticles were fixed on the grid. The images were processed in the DigitalMicrograph software, measuring more than 200 nanoparticles to evaluate the particle size distribution.

The magnetic properties of the nanoparticles were studied from magnetization measurements performed on a Quantum Design MPMS SQUID magnetometer. The magnetization (M) was measured as a function of the temperature (T), between 5 and 320 K, applying a magnetic field (H) of 10 Oe, in the zero-field-cooled (ZFC) and field-cooled (FC) modes. The magnetization measurements as a function of the applied magnetic field were carried out at 5 and 320 K, by applying a magnetic field of up to 55 kOe. These two measurement temperatures were selected because they correspond to the extremes of the temperature range in which the magnetometer used operates. M vs. H measurements at other temperatures were not performed because, after analyzing the temperature dependence of magnetization, no variations or points of interest were observed on the curves. From the M vs. H curves, parameters such as the coercive field (H_C), the saturation magnetization (M_S) and the remanent magnetization (M_R) were determined.

III. Results and Discussion

In Fig. 1, the X-ray diffractograms of the synthesized $Co_{1-x}Ni_xFe_2O_4$ (x = 0.0, 0.2, 0.4, and 0.5) nanoparticles are shown, in addition to the XRD pattern of $CoFe_2O_4$ (JCPDS: 22-1086). All the peaks observed in the diffractograms are identified in the standard XRD pattern of cobalt ferrite, indicating that the four synthesized compounds present a single crystalline phase corresponding to the cubic spinel structure.

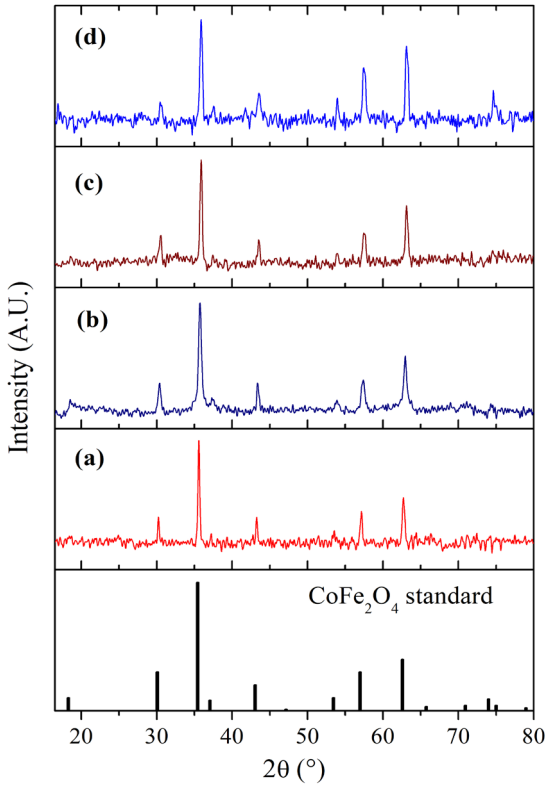

Fig. 1 Standard XRD pattern of the cobalt ferrite and X-ray diffractograms of the synthesized nanoparticles of (a) $CoFe_2O_4$, (b) $Co_{0.8}Ni_{0.2}Fe_2O_4$, (c) $Co_{0.6}Ni_{0.4}Fe_2O_4$, and (d) $Co_{0.5}Ni_{0.5}Fe_2O_4$.

The diffraction peaks of small intensities found in the XRD pattern of Co fe rrite could not be identified in the diffractograms of the synthesized powder samples, because they are hidden in the background of the measurements, which can be attributed to the small size of the crystalline domains, the same reason that the broadening of the diffraction peaks is generated in nanoparticulate materials [21].

When reviewing in detail the diffractograms of Fig. 1, a slight shift of the diffraction peaks towards a greater 2θ angle is observed, as the Ni content in the ferrite increases. This shift is evident in the values of $2\theta_{obs}$ that are tabulated in Table I, which is due to the fact that the Ni^{2+} cations are smaller than those of Co^{2+}, with the radii of these ions being 0.72 and 0.78 Å, respectively [22], [23]. Table I also shows the indexing of the seven diffraction peaks observed in the diffractograms, identifying the peak with the highest intensity as the one corresponding to the (3 1 1) crystallographic planes.

TABLE I
INDEXING (H K L) OF THE MAXIMUM DIFFRACTION PEAKS OBSERVED IN THE DIFFRACTOGRAMS OF THE SYNTHESIZED FERRITE NANOPARTICLES

Ferrite	h k l - $2\theta_{obs}$ (°)						
	2 2 0	3 1 1	2 2 2	4 0 0	4 2 2	5 1 1	4 4 0
$CoFe_2O_4$	30.25	35.60	37.20	43.25	53.55	57.15	62.70
$Co_{0.8}Ni_{0.2}Fe_2O_4$	30.27	35.66	36.85	43.30	53.69	57.25	62.60
$Co_{0.6}Ni_{0.4}Fe_2O_4$	30.52	35.90	37.45	43.53	53.95	57.47	63.12
$Co_{0.5}Ni_{0.5}Fe_2O_4$	30.39	35.80	37.35	43.50	53.79	57.40	63.23

Table II shows the values of the unit cell parameter calculated for the four ferrites under study. It is observed that as Co is replaced by Ni in the cobalt ferrite, a decrease in the lattice parameter is generated, which is due to the fact that Ni^{2+} cations are smaller than Co^{2+} cations. In the case of $Co_{0.5}Ni_{0.5}Fe_2O_4$, a difference was found in the trend of change of the unit cell parameter, since the value of *a* is slightly higher than that of $Co_{0.6}Ni_{0.4}Fe_2O_4$, which may be due to the redistribution of cations between the tetrahedral and octahedral sites of the spinel structure, since half of the ions are Ni^{2+} and these have a preference for being located in the octahedral sites, while Co^{2+} is located in both tetrahedral and octahedral sites. The value of the unit cell parameter of the synthesized cobalt ferrite is lower than that of the $CoFe_2O_4$ standard (JCPDS: 22-1086), however, it is within the values reported in the literature that vary between 8.36 and 8.40 Å [24], [25].

TABLE II
UNIT CELL PARAMETER AND MEAN PARTICLE SIZE OF THE SYNTHESIZED FERRITE NANOPARTICLES

Ferrite	Unit cell parameter, *a* (Å)	Mean particle size, *D* (nm)
$CoFe_2O_4$	8.362 (4)	42
$Co_{0.8}Ni_{0.2}Fe_2O_4$	8.348 (3)	38
$Co_{0.6}Ni_{0.4}Fe_2O_4$	8.284 (4)	37
$Co_{0.5}Ni_{0.5}Fe_2O_4$	8.321 (5)	34

Fig. 2 shows the TEM images of the four synthesized ferrites, where it is observed that all the compounds are formed by irregularly shaped nanoparticles, which are agglomerated. In Fig. 3 the particle size histograms of the four synthesized compounds are shown, where it is evident that all the ferrites

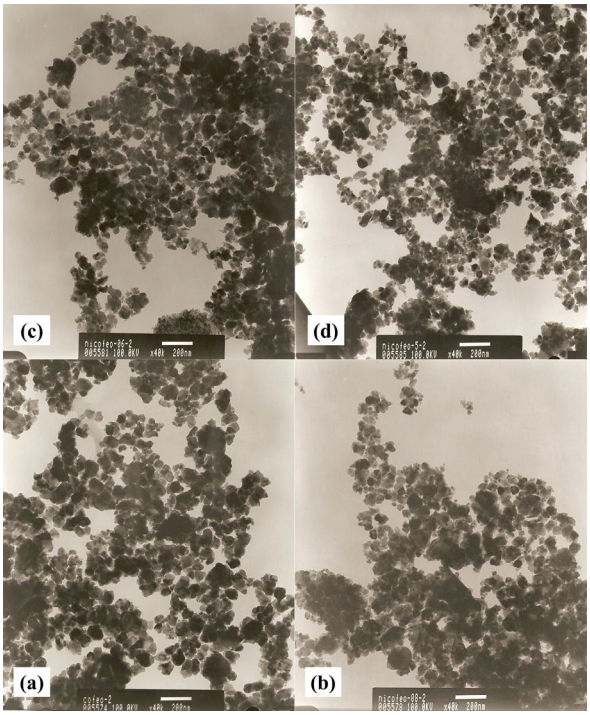

Fig. 2 TEM images of the synthesized nanoparticles of (a) $CoFe_2O_4$, (b) $Co_{0.8}Ni_{0.2}Fe_2O_4$, (c) $Co_{0.6}Ni_{0.4}Fe_2O_4$, and (d) $Co_{0.5}Ni_{0.5}Fe_2O_4$. The scale bar in all micrographs corresponds to 200 nm.

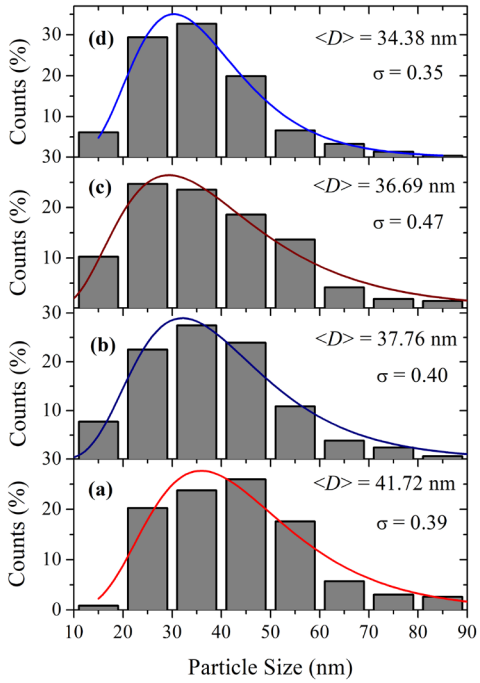

Fig. 3 Size histograms of the synthesized nanoparticles of (a) $CoFe_2O_4$, (b) $Co_{0.8}Ni_{0.2}Fe_2O_4$, (c) $Co_{0.6}Ni_{0.4}Fe_2O_4$, and (d) $Co_{0.5}Ni_{0.5}Fe_2O_4$.

have wide size distributions with nanoparticles ranging from 15 nm to 85 nm. The particle size distributions are of the Log-normal type, with standard deviations between 0.35 and 0.47, and mean particle sizes between 34 and 42 nm. The mean particle sizes of each compound are tabulated in Table II, and are similar to those reported in other investigations where nanoparticulate powders have been produced by similar synthesis routes and where the powders have been calcined at temperatures between 600 and 800°C [15], [20].

Fig. 4 shows the magnetization curves as a function of temperature, in ZFC and FC modes, for $CoFe_2O_4$ and $Co_{0.5}Ni_{0.5}Fe_2O_4$ ferrites, where it is observed that the magnetic response of materials depends on the previous cooling in the absence or in the presence of an applied magnetic field. The irreversibility of the magnetization observed over the entire measurement temperature range suggests that the nanoparticles of both compounds are in the blocked regime between 5 and 320 K, that is, at temperatures below 320 K both nanocompounds present a collective magnetic response where the particle magnetic moments are blocked [26].

With the reduction of thermal energy, it is expected that the magnetic moments align in the direction of the applied magnetic field, generating the increase in magnetization as the temperature is reduced; however, in the FC curves it is observed that the magnetization decreases with the reduction of the temperature, which is due to strong magnetic interactions between the nanoparticles, which oppose the ordering of magnetic moments as a result of the application of an external magnetic field. The existence of interparticle magnetic interactions is consistent with what was observed in the TEM micrographs, where it was evidenced that the nanoparticles are found together forming particle aggregates. When comparing the magnetization curves of the two materials, it is observed that $CoFe_2O_4$ presents a greater magnetic response than Co-Ni mixed ferrite, a result that is obvious because Co^{2+} ions have a greater magnetic moment than Ni^{2+} cations, being 3 and 2 μ_B, respectively [27].

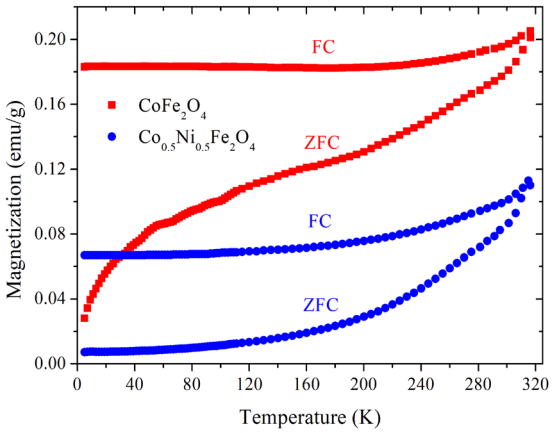

Fig. 4 Temperature dependence of the ZFC and FC magnetizations, with H = 10 Oe, of $CoFe_2O_4$ and $Co_{0.5}Ni_{0.5}Fe_2O_4$ nanoparticles.

Fig. 5 shows the magnetization curves as a function of the applied magnetic field, measured at 5 and 320 K, for $CoFe_2O_4$ and $Co_{0.5}Ni_{0.5}Fe_2O_4$ ferrites, where it is observed that at both temperatures the two compounds exhibit magnetic hysteresis. In the inset of Fig. 5(b) it is evident that at 320 K the two nanoferrites present an irreversible magnetization process, with non-zero coercive fields. These results confirm that, in the temperature range between 5 and 320 K, the nanoparticles of both compounds are in the blocked magnetic regime.

In all the hysteresis curves it is observed that the magnetic saturation state was not achieved with the maximum applied magnetic field applied, therefore the values of the saturation magnetization (M_S) were estimated by means of the infinite field approximation; for this, an extrapolation to infinite field of the magnetization data plotted as a function of $1/H$ was carried out, in the high field range, and the equation $M = M_S\,(1 - \beta/H)$ was used, where β is a magnetic field-independent parameter [20].

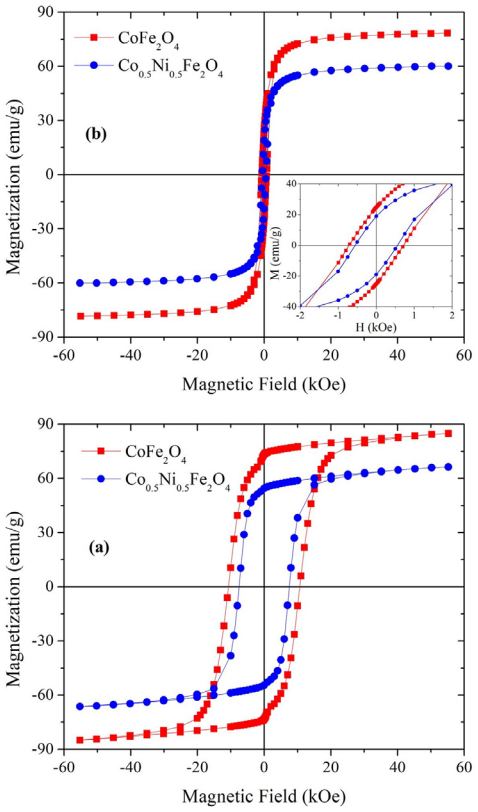

Fig. 5 Magnetic field dependence of magnetization, measured at (a) 5 K and (b) 320 K, of $CoFe_2O_4$ and $Co_{0.5}Ni_{0.5}Fe_2O_4$ nanoparticles. The inset in (b) shows the $M(H)$ curves at 320 K in the region of a small applied field.

Table III shows the values of the saturation magnetization, the remanent magnetization, and the coercive field of the two nanocompounds, at both measurement temperatures. A decrease in the values of the three magnetic parameters with increasing temperature is evident, however, both M_R and H_C are still large at 320 K, which indicates that at this temperature the nanoparticles are blocked presenting an ordered magnetic behavior as a response to the application of an external magnetic field. The M_S values are also large and result from the alignment of the magnetic moments of the particles (μ_p) in the

direction of H. These μ_p are the result of the internal ordering of the cationic magnetic moments that form the nanoparticles, which must be the characteristic ferrimagnetic ordering of spinel ferrites [10], [28].

When comparing the hysteresis curves of the two materials, it is found that the values of M_S, M_R and H_C decrease with the incorporation of Ni, which is due to the reduction in the amount of Co^{2+} cations, which have a greater magnetic moment than that of the divalent cations of Ni. The M_S and H_C values of cobalt ferrite are among the highest values reported in the literature for nanoparticles of this oxide synthesized by methods such as sol-gel or aerosol [24], [29]. The M_S values obtained at 5 and 320 K, for $Co_{0.5}Ni_{0.5}Fe_2O_4$ nanoparticles, are higher than those reported in the literature for Ni ferrite, both in its nanoparticulate and bulk form, which vary between 54 and 56 emu/g (at $T \leq 5$ K), and between 47 and 50 emu/g (at $T \sim 300$ K) [27], [30]. In addition, the saturation magnetization and coercive field values of $Co_{0.5}Ni_{0.5}Fe_2O_4$ ferrite nanoparticles, obtained at 320 K, are close to those reported in other investigations ($63.35 \leq M_S \leq 67.30$ emu/g, $124 \leq H_C \leq 565$ Oe) where they have studied the magnetic properties, at room temperature, of Co-Ni mixed ferrite nanoparticles synthesized by other methods such as sol-gel [31], [32].

TABLE III
SATURATION MAGNETIZATION (M_S), REMANENT MAGNETIZATION (M_R), AND COERCIVE FIELD (H_C), MEASURED AT 5 AND 320 K, OF THE SYNTHESIZED FERRITE NANOPARTICLES

Ferrite	T_{meas} (K)	M_S (emu/g)	M_R (emu/g)	H_C (Oe)
$CoFe_2O_4$	5	87.33	73.29	10683
	320	79.79	24.95	720
$Co_{0.5}Ni_{0.5}Fe_2O_4$	5	68.99	54.56	7518
	320	61.47	18.96	555

IV. CONCLUSION

Using the coprecipitation method, it was possible to synthesize nanoparticulate powders of $CoFe_2O_4$, $Co_{0.8}Ni_{0.2}Fe_2O_4$, $Co_{0.6}Ni_{0.4}Fe_2O_4$ and $Co_{0.5}Ni_{0.5}Fe_2O_4$ ferrites, which presented average particle sizes between 34 and 42 nm. The synthesized compounds have good crystallinity and only presented a crystalline phase corresponding to the cubic spinel structure. The substitution of Co by Ni in the cobalt ferrite generated a decrease in the lattice parameter that is associated with the fact that Ni^{2+} cations have a smaller size than Co^{2+} cations. The compounds are formed by aggregates of nanoparticles, which favors the existence of strong magnetic interactions between the particles, which are in the blocked magnetic regime in the temperature range between 5 and 320 K. As Co is replaced by Ni, it is found that the magnetic response is reduced and the values of the magnetic parameters decrease, because the magnetic moments of Ni^{2+} are smaller than those of Co^{2+}.

ACKNOWLEDGMENT

The authors thank Giovanni Attolini and Fulvio Bolzoni, from IMEM-CNR, in Parma - Italy, for their collaboration with XRD and SQUID magnetometry measurements, respectively. In addition, thanks to the Polymers Group of the Simón Bolívar University (USB), in Venezuela, for their support with the TEM images.

REFERENCES

[1] A. Mahmood and A. Maqsood, "High-frequency dielectric response of 3d metal (Mn and Cu) doped zinc ferrite nanoparticles for microwave applications," *Mater. Today Commun.*, vol. 34, p. 105042, Mar. 2023, doi: 10.1016/j.mtcomm.2022.105042.

[2] F. A. Sheikh *et al.*, "Dielectrically modified Dy^{3+} substituted nickel-cobalt ferrites for high frequency devices," *Phys. B Condens. Matter*, vol. 652, p. 414656, Mar. 2023, doi: 10.1016/j.physb.2023.414656.

[3] S. Hazra and N. N. Ghosh, "Preparation of Nanoferrites and Their Applications," *J. Nanosci. Nanotechnol.*, vol. 14, no. 2, pp. 1983–2000, 2014, doi: 10.1166/jnn.2014.8745.

[4] Y. K. Fetisov, D. Chashin, and L. Fetisov, "Magnetoelectric Ferrite–Piezoelectric Heterostructure With Coil-Free Excitation for DC Magnetic Field Sensing," *IEEE Sensors Lett.*, vol. 5, no. 11, pp. 1–4, Nov. 2021, doi: 10.1109/LSENS.2021.3123099.

[5] M. I. A. Abdel Maksoud *et al.*, "Engineered magnetic oxides nanoparticles as efficient sorbents for wastewater remediation: a review," *Environ. Chem. Lett.*, vol. 20, no. 1, pp. 519–562, Feb. 2022, doi: 10.1007/s10311-021-01351-3.

[6] D. Singh and B. R. Gurjar, "Recent innovation and impacts of nano-based technologies for wastewater treatment on humans: a review," *Environ. Monit. Assess.*, vol. 195, no. 3, p. 357, Mar. 2023, doi: 10.1007/s10661-022-10790-6.

[7] Y. F. Shen, J. Tang, Z. H. Nie, Y. D. Wang, Y. Ren, and L. Zuo, "Tailoring size and structural distortion of Fe_3O_4 nanoparticles for the purification of contaminated water.," *Bioresour. Technol.*, vol. 100, no. 18, pp. 4139–46, Sep. 2009, doi: 10.1016/j.biortech.2009.04.004.

[8] S. Keshri and S. Biswas, "Synthesis, physical properties, and biomedical applications of magnetic nanoparticles: a review," *Prog. Biomater.*, vol. 11, no. 4, pp. 347–372, Dec. 2022, doi: 10.1007/s40204-022-00204-8.

[9] V. F. Cardoso, A. Francesko, C. Ribeiro, M. Bañobre-López, P. Martins, and S. Lanceros-Mendez, "Advances in Magnetic Nanoparticles for Biomedical Applications," *Adv. Healthc. Mater.*, vol. 7, no. 5, pp. 1–35, 2018, doi: 10.1002/adhm.201700845.

[10] D. S. Mathew and R.-S. Juang, "An overview of the structure and magnetism of spinel ferrite nanoparticles and their synthesis in microemulsions," *Chem. Eng. J.*, vol. 129, no. 1–3, pp. 51–65, May 2007, doi: 10.1016/j.cej.2006.11.001.

[11] T. A. S. Ferreira, J. C. Waerenborgh, M. H. R. M. Mendonça, M. R. Nunes, and F. M. Costa, "Structural and morphological characterization of $FeCo_2O_4$ and $CoFe_2O_4$ spinels prepared by a coprecipitation method," *Solid State Sci.*, vol. 5, no. 2, pp. 383–392, Feb. 2003, doi: 10.1016/S1293-2558(03)00011-6.

[12] I. Sharifi, H. Shokrollahi, and S. Amiri, "Ferrite-based magnetic nanofluids used in hyperthermia applications," *J. Magn. Magn. Mater.*, vol. 324, no. 6, pp. 903–915, Mar. 2012, doi: 10.1016/j.jmmm.2011.10.017.

[13] S. A. Majetich, T. Wen, and O. T. Mefford, "Magnetic nanoparticles," *MRS Bull.*, vol. 38, no. 11, pp. 899–903, 2013, doi: 10.1557/mrs.2013.230.

[14] F. Morales, G. Márquez, V. Sagredo, T. E. Torres, and J. C. Denardin, "Structural and magnetic properties of silica-coated magnetite nanoaggregates," *Phys. B Condens. Matter*, vol. 572, pp. 214–219, Nov. 2019, doi: 10.1016/j.physb.2019.08.007.

[15] E. Pérez, G. Márquez, and V. Sagredo, "Effect of Calcination on Characteristics of Nickel Ferrite Nanoparticles Synthesized by Sol- Gel Method," *Iraqi J. Appl. Phys.*, vol. 15, no. 1, pp. 13–17, 2019.

[16] P. Samoila *et al.*, "Cobalt Ferrite Particles Produced by Sol-Gel Autocombustion and Embedded in Polysilane: An Innovative Route to Magnetically-Induced Fluorescence Composites," *Molecules*, vol. 27, no. 19, p. 6393, Sep. 2022, doi: 10.3390/molecules27196393.

[17] N. K. Chandra Babu, S. Prathap, and W. Madhuri, "Effect of Microwave Heat Treatment on Hydrothermal Synthesis of Nano-$MgFe_2O_4$," *J. Supercond. Nov. Magn.*, vol. 33, no. 2, pp. 417–425, Feb. 2020, doi: 10.1007/s10948-019-05194-6.

[18] H. M. Noor ul Huda Khan Asghar *et al.*, "Structural and magnetic properties of Co–Cd–Zn spinel ferrite nanoparticles synthesized through

micro-emulsion method," *Opt. Quantum Electron.*, vol. 53, no. 12, p. 677, Dec. 2021, doi: 10.1007/s11082-021-03299-8.
[19] M. M. Baig *et al.*, "Structural and electrical properties of La^{3+} ions substituted $MnFe_2O_4$ ferrite nanoparticles synthesized via cost-effective reverse micelles strategy," *Mater. Res. Express*, vol. 8, no. 3, p. 035002, Mar. 2021, doi: 10.1088/2053-1591/abd73b.
[20] G. Márquez, V. Sagredo, R. Guillén-Guillén, G. Attolini, and F. Bolzoni, "Calcination effects on the crystal structure and magnetic properties of $CoFe_2O_4$ nanopowders synthesized by the coprecipitation method," *Rev. Mex. Física*, vol. 66, no. 3 May-Jun, p. 251, May 2020, doi: 10.31349/RevMexFis.66.251.
[21] D. P. Shaik, R. Pitcheri, Y. Qiu, and O. M. Hussain, "Hydrothermally synthesized porous Mn_3O_4 nanoparticles with enhanced electrochemical performance for supercapacitors," *Ceram. Int.*, vol. 45, no. 2, pp. 2226–2233, Feb. 2019, doi: 10.1016/j.ceramint.2018.10.135.
[22] P. A. Shaikh, R. C. Kambale, A. V. Rao, and Y. D. Kolekar, "Structural, magnetic and electrical properties of Co-Ni-Mn ferrites synthesized by co-precipitation method," *J. Alloys Compd.*, vol. 492, no. 1–2, pp. 590–596, 2010, doi: 10.1016/j.jallcom.2009.11.189.
[23] E. Santiago, G. Marquez, R. Guillen-Guillen, C. Jaimes, V. Sagredo, and G. E. Delgado, "Characterization of hematite and Ni-Zn mixed ferrites nanocomposites synthesized by the coprecipitation method," *Rev. Latinoam. Metal. y Mater.*, vol. 40, no. 1, pp. 49–58, 2020, [Online]. Available: http://www.rlmm.org/ojs/index.php/rlmm/article/view/984.
[24] T. Meron, Y. Rosenberg, Y. Lereah, and G. Markovich, "Synthesis and assembly of high-quality cobalt ferrite nanocrystals prepared by a modified sol–gel technique," *J. Magn. Magn. Mater.*, vol. 292, pp. 11–16, Apr. 2005, doi: 10.1016/j.jmmm.2004.10.084.
[25] P. C. Rajath Varma, R. Sekhar Manna, D. Banerjee, M. Raama Varma, K. G. Suresh, and A. K. Nigam, "Magnetic properties of $CoFe_2O_4$ synthesized by solid state, citrate precursor and polymerized complex methods: A comparative study," *J. Alloys Compd.*, vol. 453, no. 1–2, pp. 298–303, Apr. 2008, doi: 10.1016/j.jallcom.2006.11.058.
[26] M. Knobel, W. C. Nunes, L. M. Socolovsky, E. De Biasi, J. M. Vargas, and J. C. Denardin, "Superparamagnetism and Other Magnetic Features in Granular Materials: A Review on Ideal and Real Systems," *J. Nanosci. Nanotechnol.*, vol. 8, no. 6, pp. 2836–2857, Apr. 2008, doi: 10.1166/jnn.2008.017.
[27] B. D. Cullity and C. D. Graham, *Introduction to Magnetic Materials*, 2nd ed. New York: IEEE Press, 2009.
[28] S. Mørup, M. F. Hansen, and C. Frandsen, "Magnetic Nanoparticles," in *Comprehensive Nanoscience and Technology*, Elsevier, 2011, pp. 437–491.
[29] S. Singhal, J. Singh, S. . Barthwal, and K. Chandra, "Preparation and characterization of nanosize nickel-substituted cobalt ferrites ($Co_{1-x}Ni_xFe_2O_4$)," *J. Solid State Chem.*, vol. 178, no. 10, pp. 3183–3189, Oct. 2005, doi: 10.1016/j.jssc.2005.07.020.
[30] G. Márquez, V. Sagredo, and R. Guillén-Guillén, "Structural Characterization, Magnetic Properties, and Heating Power of Nickel Ferrite Nanoparticles," *IEEE Trans. Magn.*, vol. 55, no. 12, pp. 1–7, Dec. 2019, doi: 10.1109/TMAG.2019.2939118.
[31] O. H. Mohammed, A. S. Jassim, and S. J. Fathi, "Effect of laser on magnetic properties of nano composite material ($Ni_{0.5}Co_{0.5}Fe_2O_4$) prepared by sol–gel," *Mater. Today Proc.*, vol. 61, pp. 921–924, 2022, doi: 10.1016/j.matpr.2021.10.099.
[32] J. Sun, J. Chen, H. Ge, H. Sun, Y. Yang, and Y. Zhang, "Biomass-derived carbon decorated with $Ni_{0.5}Co_{0.5}Fe_2O4$ particles towards excellent microwave absorption performance," *Compos. Part A Appl. Sci. Manuf.*, vol. 156, no. November 2021, p. 106850, 2022, doi: 10.1016/j.compositesa.2022.106850.